Universal off-diagonal long-range-order behavior for a trapped Tonks-Girardeau gas

A. Colcelli,[1] J. Viti,[2] G. Mussardo,[1] and A. Trombettoni[3,1]
[1]*SISSA and INFN, Sezione di Trieste, Via Bonomea 265, I-34136 Trieste, Italy*
[2]*International Institute of Physics & ECT, UFRN, Campos Universitário, Lagoa Nova 59078-970 Natal, Brazil*
[3]*CNR-IOM DEMOCRITOS Simulation Center, Via Bonomea 265, I-34136 Trieste, Italy*

(Received 21 September 2018; published 26 December 2018)

The scaling of the largest eigenvalue λ_0 of the one-body density matrix of a system with respect to its particle number N defines an exponent $\mathcal{C}$ and a coefficient $\mathcal{B}$ via the asymptotic relation $\lambda_0 \sim \mathcal{B}\, N^{\mathcal{C}}$. The case $\mathcal{C} = 1$ corresponds to off-diagonal long-range order. For a one-dimensional homogeneous Tonks-Girardeau gas, a well-known result also confirmed by bosonization gives instead $\mathcal{C} = 1/2$. Here we investigate the inhomogeneous case, initially addressing the behavior of $\mathcal{C}$ in the presence of a general external trapping potential V. We argue that the value $\mathcal{C} = 1/2$ characterizes the hard-core system independently of the nature of the potential V. We then define the exponents γ and β, which describe the scaling of the peak of the momentum distribution with N and the natural orbital corresponding to λ_0, respectively, and we derive the scaling relation $\gamma + 2\beta = \mathcal{C}$. Taking as a specific case the power-law potential $V(x) \propto x^{2n}$, we give analytical formulas for γ and β as functions of n. Analytical predictions for the coefficient $\mathcal{B}$ are also obtained. These formulas are derived by exploiting a recent field theoretical formulation and checked against numerical results. The agreement is excellent.

DOI: 10.1103/PhysRevA.98.063633

I. INTRODUCTION

The one-body density matrix (OBDM) $\rho(x, y)$ is a quantity of central importance for the statistical properties of interacting quantum systems. In a second quantized formalism for a many-body bosonic system it can be written as the one-particle correlation function

$$\rho(x, y) = \langle \Omega | \Psi^\dagger(x) \Psi(y) | \Omega \rangle, \tag{1}$$

where Ψ and $\Psi^\dagger$ are bosonic field operators and $|\Omega\rangle$ is the many-body ground state. The eigenvalues λ_j of the OBDM are defined by the solution of the integral equation

$$\int dy\, \rho(x, y)\, \varphi_j(y) = \lambda_j\, \varphi_j(x)\,, \tag{2}$$

where the functions φ_j are usually called natural orbitals [1]. The scaling of the largest eigenvalue λ_0 of (2) with respect to the total number N of particles gives information on whether the system exhibits off-diagonal long-range order (ODLRO) and, as a consequence of the Penrose-Onsager criterion, Bose-Einstein condensation [2,3]. Indeed, in the presence of ODLRO, the OBDM has nonvanishing off-diagonal elements, which implies for a homogeneous system a Dirac δ peak in the momentum distribution. This means that one has a macroscopic occupation of the lowest energy state, therefore making λ_0 scale with N, i.e., $\lambda_0 = O(N)$. On the other hand, when all the eigenvalues of $\rho(x, y)$ in Eq. (2) are order 1, the system exhibits fermionic behavior, obeying the Pauli exclusion principle.

Intermediate situations may arise, however, in one-dimensional (1D) systems: Even though in such systems quantum fluctuations strongly deplete (and in the thermodynamic limit completely prevent) the Bose-Einstein condensate, the lowest eigenvalue of the OBDM nevertheless scales in a nontrivial way with respect to N, not being of order 1. When N is large, it is possible to define an exponent $\mathcal{C}$ via the relation

$$\lambda_0 \sim \mathcal{B} N^{\mathcal{C}}. \tag{3}$$

Continuous variations of the exponent $\mathcal{C}$ give rise to a whole spectrum of possible order types—long-range order, midrange order, and short-range order—as discussed in [4]. For one-dimensional bosons with a two-body δ interaction, i.e., the Lieb-Liniger model [5], and in the absence of an external one-body trapping potential $V(x)$, the dependence of the exponent $\mathcal{C}$ on the interaction strength and the density of particles has been studied in [6]. In this homogeneous case, denoting by γ the coupling constant of the Lieb-Liniger model, in the weakly interacting limit $\gamma \to 0$ we have $\mathcal{C} \to 1$, while in the strong-coupling regime $\gamma \to \infty$ we have $\mathcal{C} \to 1/2$, both results in agreement with bosonization [7,8]. The limit of infinite γ corresponds to the Tonks-Girardeau (TG) gas [9], i.e., 1D hard-core bosons, and the result $\mathcal{C} = 1/2$ [10] confirms the nature of the TG gas as intermediate between bosons and fermions, despite the fact that one-point observables are identical to those of fermions [11].

The definition of ODLRO, related to the long-distance behaviors of the OBDM, is, of course, valid both for homogeneous [$V(x) = 0$] and inhomogeneous [$V(x) \neq 0$] systems. However, besides the inherent difficulty of dealing with interacting systems (which is also present for the homogeneous systems), the study of the large-N limit in the presence of an external trapping potential shows several additional difficulties due to the lack of translational invariance. For instance: (i) numerical methods working at small N may not be able to give the correct large-N behavior; (ii) the presence of the potential V may spoil the validity of methods which explicitly exploit the translational invariance of the system,

such as the perturbative expansions done in terms of Feynman diagrams in momentum space; and (iii) for 1D systems, the external trapping potential typically also breaks the integrability of the homogeneous limit. Although one could derive useful information from approaches based on local density approximation, a complete study of the ODLRO behavior of strongly correlated quantum systems in the presence of external trapping potentials remains a challenging task.

With this main motivation, in this paper we focus on the characterization of the ODLRO in a TG gas at $T = 0$ in the presence of external trapping potentials. The interest in such a study relies both on the experimental and theoretical sides. Indeed, much progress have been made in realizing the TG gas with ultracold atoms and characterizing its properties, such as momentum distribution and ground-state energy [12,13]. For the TG gas, one can also study the confinement of induced resonances as well as the crossover to the so-called super-TG gas [14]; in the presence of a periodic potential, one can also address the quantum phase transition which induces to a Mott insulating state [15,16]. From a theoretical perspective, one is able to work out analytical results for this system thanks to its integrability [17,18] and the Bose-Fermi equivalence [19,20], which permits us to map the TG gas into a system of noninteracting spinless fermions. It is also known that for a trapped TG gas one can write a closed expression for the OBDM [21]. For all these reasons there is a broad interest in the study of correlation functions of the TG gas in different potentials, such as harmonic traps [22–28], optical lattices [29–35], disordered potentials [36–38], or also of the super-TG state [39–43]. (See [44] for additional references.) The effects of an harmonic confinement were studied also for hard-core anyons, whose limit of vanishing statistical parameters gives the TG gas [45,46].

In the presence of a trapping potential, there are two ways in which one can take the large-N limit: (a) increasing N and at the same time varying the parameters of the external potential V (e.g., the harmonic oscillator length for the harmonic potential) in such a way to keep the density at the center of the trap fixed, for instance; (b) or fixing the parameters of the external potential V and simply increasing N. It turns out that the scaling of the largest eigenvalue of the OBDM is the same in both cases (see Sec. IV B for more details).

The influence of a trapping potential on an interacting system was studied by a renormalization group approach in [47], where the effects of the trap inhomogeneity on the critical behavior can be cast in the form of a trap-size scaling and used to characterize trapped systems undergoing quantum phase transitions [48]. The TG gas does not exhibit phase transitions at variance, and our goal is to study the effects at zero temperature of the varying trapping potential, increasing the particle number, or fixing the density at the center of the trap.

In this paper we first show that the result $\mathcal{C} = 1/2$ holds for a TG gas independently of the external potential V. We will argue that the universality of this result can be predicted by exploiting the expression of the OBDM of a TG gas in a generic trapping potential obtained in [49]. Such an expression that is valid for large N was derived by expanding a conformal field theory (CFT) approach introduced in [50].

We then discuss the emergence of other power-law behaviors for the Tonks-Girardeau gas. Suitably rescaling the space coordinate x, as explained in detail in Sec. IV, one can study how the peak at zero momentum of the dimensionful momentum distribution $\tilde{\rho}(k)$ and the natural orbital φ_0 corresponding to λ_0 scale with the particle number. These two quantities respectively define two exponents, denoted by γ and β, which we will show are related via $\gamma + 2\beta = \mathcal{C}$. For simplicity, we will mainly refer to power-law potentials of the form $V(x) \propto x^{2n}$, interpolating between the harmonic potential ($n = 1$) and the hard wall trap ($n \to \infty$). For these power-law potentials we are able to predict the dependence on n of both γ and β. We are also able to obtain accurate predictions for the coefficient $\mathcal{B}$ that appears as a prefactor in the scaling relation (3). We corroborate these results using both a WKB approximation and direct numerical calculations. Finally, we obtain the scaling with the particle number of the dimensionful momentum distribution peak. The latter is characterized by the same exponent $1/2$, irrespective of the external potential, in analogy with the result for the largest eigenvalue λ_0.

The paper is organized as follows. In Sec. II we revisit the OBDM of a TG gas and derive its expression in terms of the single-particle wave functions of the system [21]. In Sec. III, we discuss the scaling behavior for the largest eigenvalue of the OBDM and the peak of the momentum distribution, as well as a relation among these exponents. In Sec. IV we present a numerical study of the scaling of λ_0 and n_{peak} with respect to N. Our main results are reported in Table V. We finally gather our conclusions in Sec. V, while some details about the numerical methods are reported in Appendix A.

II. THE MODEL AND ITS ONE-BODY DENSITY MATRIX

In the limit of infinite coupling, the Lieb-Liniger model reduces to a system of N impenetrable bosons of mass m. Such a system is known as the TG gas [9], and it is described by the Schrödinger equation

$$H\,\psi(x_1, \ldots, x_N) = E\,\psi(x_1, \ldots, x_N), \tag{4}$$

where the Hamiltonian is written as a sum of single-particle Hamiltonians

$$H = \sum_{i=1}^{N} \left[-\frac{\hbar^2}{2m} \frac{\partial^2}{\partial x_i^2} + V(x_i) \right]. \tag{5}$$

In (4) the many-body wave functions ψ are symmetric in the exchange of two coordinates due to the bosonic statistics, although they vanish when two arguments have the same value for the hard-core interactions,

$$\psi|_{x_i = x_j} = 0\,, \quad \forall i \neq j = 1, \ldots, N. \tag{6}$$

The many-body wave functions of the system can then be written in a Slater determinant form by adding sign functions to ensure the correct symmetry under coordinate exchange,

$$\psi(x_1, \ldots, x_N) = \frac{1}{\sqrt{N!}} \det \left[\phi_k(x_l) \right]_{\substack{k = 0, \ldots, N-1, \\ l = 1, \ldots, N}} \times \prod_{1 \leqslant i < j \leqslant N} \operatorname{sgn}(x_i - x_j). \tag{7}$$

This is the content of the well-known Fermi-Bose equivalence [19,20], where $\phi_k(x)$ denotes the kth eigenfunction of the single-particle Schrödinger equation ($k = 0, \ldots, N-1$),

$$\left[-\frac{\hbar^2}{2m}\frac{d^2}{dx^2} + V(x)\right]\phi_k(x) = \varepsilon_k \phi_k(x), \tag{8}$$

and ε_k is the corresponding single-particle energy.

The Hermitian OBDM $\rho(x, y)$ of the 1D quantum gas is defined as

$$\rho(x, y) = N \int \prod_{i=2}^{N} dx_i \psi^*(x, x_2, \ldots, x_N) \times \psi(y, x_2, \ldots, x_N). \tag{9}$$

Notice that $\rho(x, y)$ is also often referred to in literature (for instance, [51]) as $g_1(x, y)$. In the following, the integrals are meant to be between $-\infty$ and $+\infty$ each time that their extremes are not explicitly written.

The solutions of the eigenvalue equation for the OBDM, i.e., Eq. (2), involve the natural orbitals $\varphi_j(x)$: They represent the effective single-particle states of the system, while the $\phi_k(x)$ can be viewed as the natural orbitals for the ideal fermionic gas [52]. The natural orbitals are chosen to be orthonormal, $\int dx\, \varphi_i^*(x)\varphi_j(x) = \delta_{ij}$. The occupation numbers of the levels j, expressed by λ_j, satisfy the normalization condition

$$\sum_j \lambda_j = N, \tag{10}$$

which is a consequence of $\int dx\, \rho(x, x) = N$. By substituting Eq. (7) into Eq. (9) and expanding the Slater determinants along the first column, we obtain

$$\rho(x, y) = \frac{1}{(N-1)!}\sum_{i,j=0}^{N-1}(-1)^{i+j}\,\phi_i(y)\,\phi_j^*(x) \times \int dx_2 \ldots \int dx_N \det[f_k(x_r)]_{\substack{k=0,\ldots,N-1,\,k\neq i \\ r=2,\ldots,N}} \times \det[g_l(x_r)]_{\substack{l=0,\ldots,N-1,\,l\neq j \\ r=2,\ldots,N}}, \tag{11}$$

where $f_k(x_r) = \phi_k(x_r)\,\mathrm{sgn}(x - x_r)$, $g_l(x_r) = \phi_l^*(x_r)\,\mathrm{sgn}(y - x_r)$, with the index $k \neq i$ in the first determinant while $l \neq j$ in the second. It is worth recalling the Andréief formula (see [53] for a nice recent historical note),

$$\int dx_1 \cdots \int dx_N \det[f_j(x_k)]_{j,k=1}^N \det[g_j(x_k)]_{j,k=1}^N = N!\det\left[\int dx f_j(x) g_k(x)\right]_{j,k=1,\ldots N}, \tag{12}$$

to transform the product of two determinants in Eq. (11) into the determinant of the product. It follows that

$$\rho(x, y) = \sum_{i,j=0}^{N-1}(-1)^{i+j}\,\phi_i(y)\,\phi_j^*(x) \times \det\left[\int dt\, f_k(t) g_l(t)\right]_{k\neq i, l\neq j}. \tag{13}$$

We then substitute back in Eq. (13) the form for the functions f_k and g_l in terms of the single-particle wave functions ϕ_k, which are solutions of Eq. (8). Assuming $x > y$ and using the orthonormality condition $\int dt\, \phi_l(t)\,\phi_k^*(t) = \delta_{k,l}$, we obtain a compact form for the OBDM of a TG gas in a generic external potential $V(x)$ as

$$\rho(x, y) = \sum_{i,j=0}^{N-1}(-1)^{i+j}\,\phi_i(y)\,\phi_j^*(x) \times \det\left[\delta_{k,l} - 2\int_y^x dt\, \phi_l(t)\,\phi_k^*(t)\right]_{k\neq i, l\neq j}. \tag{14}$$

Consider now the matrix P with entries $P_{ij} = \delta_{i,j} - 2\int_y^x dt\, \phi_j(t)\,\phi_i^*(t)$, for $i, j = 0, \ldots, N-1$. From Cramér's theorem, one can check that Eq. (14) is actually equivalent to [21]

$$\rho(x, y) = \det(P)\sum_{i,j=0}^{N-1}\phi_i^*(x)\,[P^{-1}]_{ji}\,\phi_j(y), \tag{15}$$

having again assumed $x > y$ without loss of generality.

In the following, for numerical computations involving the OBDM, we find its expression given in Eq. (14) simpler to use, which does not require explicitly the inverse of the matrix P. This expression also provides a nontrivial check of the large-N limit derived in [49], as we are now going to illustrate.

III. SCALING OF λ_0 AND THE MOMENTUM DISTRIBUTION PEAK

In this section we derive our predictions for the scaling of the largest eigenvalue of the OBDM and the momentum distribution peak of a TG gas in a generic external potential by using CFT within a semiclassical framework. In this section we consider a generic trapping potential, assuming that its single-particle wave functions $\phi_j(x)$ and its natural orbitals $\varphi_j(x)$ decay fast enough at large distances. In Sec. IV we will focus on the case of an external power-law potential.

A. One-body density matrix in the semiclassical (CFT) limit

In the recent article [49], Brun and Dubail studied the large-distance behavior of the OBDM of a TG gas in a generic trapping potential and in the semiclassical limit $\hbar \to 0$, by using CFT arguments coming from a previous analysis [50]. The results of [49] were then extended in [54] to study the large-distance behavior of correlation functions of a Lieb-Liniger gas in a trap for arbitrary values of the coupling strength. Let us first briefly recall the framework and the main results of Ref. [49]. The semiclassical limit for the TG gas considered in [49] is defined as

$$\hbar \to 0, \quad \text{with } m,\ V(x),\ \mu \text{ fixed}, \tag{16}$$

where μ is the chemical potential. In the limit (16), the inhomogeneous particle density can be obtained exactly within a local density approximation as

$$\rho(x) = \frac{1}{\pi\hbar}\sqrt{2m\,[\mu - V(x)]}. \tag{17}$$

In the following we denote by x_1 and x_2 (with $x_2 > x_1$) the two solutions of the equation $\mu - V(x) = 0$ and we assume that these are the only two solutions of this equation. For $x > x_2$ or $x < x_1$ the gas density is zero and the latter is effectively confined in a spatial region $x \in [x_1, x_2]$. The total number of particles in the system is

$$N = \int_{x_1}^{x_2} \rho(x)\, dx = \frac{1}{\pi\hbar} \int_{x_1}^{x_2} \sqrt{2m\,[\mu - V(x)]}\, dx. \quad (18)$$

It follows that the $\hbar \to 0$ limit is actually the thermodynamic limit $N \to \infty$, and this gives rise to the Thomas-Fermi approximation [55]. To keep track of the leading N dependence in the limit (16), it is sufficient to observe that Eq. (18) implies

$$N\hbar = \text{const}, \quad (19)$$

i.e., $N = O(\hbar^{-1})$. The main result of [49] is an expression for the OBDM of the TG gas in Eq. (14) in the limit (16) that is valid as long as $|x - y|\rho_{\max} \gg 1$, where $\rho_{\max}$ is the maximum density in the trap. Such an expression is

$$\rho_{\rm cft}(\tilde{x}, \tilde{y}) = \sqrt{\frac{m}{2\hbar\widetilde{L}}}\, \frac{|C|^2 \left|\sin\left(\frac{\pi\tilde{x}}{\widetilde{L}}\right)\right|^{\frac{1}{4}} \left|\sin\left(\frac{\pi\tilde{y}}{\widetilde{L}}\right)\right|^{\frac{1}{4}}}{\left|\sin\left(\frac{\pi}{\widetilde{L}}\frac{\tilde{x}-\tilde{y}}{2}\right)\right|^{\frac{1}{2}} \left|\sin\left(\frac{\pi}{\widetilde{L}}\frac{\tilde{x}+\tilde{y}}{2}\right)\right|^{\frac{1}{2}}}, \quad (20)$$

where $|C|^2$ is a numerical coefficient which can be expressed in terms of the Barnes function $G(z)$ as $|C|^2 = \frac{G^4(3/2)}{\sqrt{2\pi}}$, and $\widetilde{L}$ is the time needed by a signal traveling with velocity v to cover the interval $[x_1, x_2]$. The signal velocity $v(x)$ depends on the position x as

$$v(x) = \sqrt{\frac{2}{m}\,[\mu - V(x)]}. \quad (21)$$

One has then

$$\widetilde{L} = \int_{x_1}^{x_2} \frac{du}{v(u)}. \quad (22)$$

In Eq. (20) $\widetilde{x}(x)$ represents the time needed to a signal emitted in x_1, with velocity (21), to reach x, i.e.,

$$\widetilde{x}(x) = \int_{x_1}^{x} \frac{du}{v(u)}. \quad (23)$$

It should be noticed that in the limit (16) the condition $|x - y|\rho_{\max} \gg 1$ is satisfied up to distances $|x - y| = O(N^{-1})$. To analyze Eq. (2) in the $\hbar \to 0$ limit, we can then safely replace $\rho(x, y)$ with Eq. (20) and restrict the integration domain to $y \in [x_1, x_2]$. By changing the integration variable to $\tilde{y}(y)$ through Eq. (23), we obtain the semiclassical limit of Eq. (2) for the largest eigenvalue of the OBDM,

$$\int_0^{\tilde{L}} d\tilde{y}\, w(\tilde{y}) \rho_{\rm cft}(\tilde{x}, \tilde{y}) \varphi_0(\tilde{y}) = \lambda_0 \varphi_0(\tilde{x}), \quad (24)$$

with $w(\tilde{y}) = 1/v(y(\tilde{y}))$. Plugging Eq. (20) into Eq. (24), we observe that the limit $\hbar \to 0$ is consistent on both sides only if $\lambda_0 = O(\hbar^{-1/2})$. Recalling Eq. (19), immediately we conclude that for $N \to \infty$,

$$\lambda_0 \sim \mathcal{B} N^{1/2}, \quad (25)$$

namely, in the limit (16), the scaling exponent $\mathcal{C}$ in Eq. (3) is $1/2$, independently of the shape of the potential. The result $\mathcal{C} = 1/2$ was found in the specific case of the harmonic potential in [22]. The numerical prefactor $\mathcal{B}$ is instead potential dependent and can be also explicitly calculated; we provide an example of such a computation in Sec. IV B. In Sec. IV C we also support numerically the validity of Eq. (25) for different potentials, both increasing N and keeping the density fixed. We will also estimate the value of the prefactor $\mathcal{B}$ directly from Eq. (14), thus providing another nontrivial check of Eq. (20), which, it is worth stressing again, was derived relying on field theoretical arguments only.

Equation (25) is intended to describe the scaling of λ_0 when the shape of the external potential is fixed and one varies N. We will see from numerical calculations that the same power-law scaling for λ_0 emerges when the density of particles in the external potential is fixed and one varies N and the trap parameters accordingly.

B. Momentum distribution

We consider here the small-k behavior of the momentum distribution $\tilde{\rho}(k)$ of the system, defined as

$$\tilde{\rho}(k) = \frac{1}{2\pi} \int dx \int dy\, \rho(x, y) e^{-i\,k\,(x-y)}. \quad (26)$$

From (2) X we have the eigendecomposition

$$\rho(x, y) = \sum_j \lambda_j\, \varphi_j^*(y)\, \varphi_j(x), \quad (27)$$

that, substituted into Eq. (26), gives

$$\tilde{\rho}(k) = \sum_j \lambda_j |\tilde{\varphi}_j(k)|^2, \quad (28)$$

where $\tilde{\varphi}_j(k) = \frac{1}{\sqrt{2\pi}} \int dx\, e^{-ikx} \varphi_j(x)$ is the Fourier transform of the natural orbital. Hence the zero-momentum distribution $n_{\rm peak} \equiv \tilde{\rho}(k = 0)$ is given by

$$n_{\rm peak} = \frac{1}{2\pi} \sum_j \lambda_j\, M_j, \quad (29)$$

where the quantities $M_j \equiv |\int dx\, \varphi_j(x)|^2$ involve the natural orbitals.

Notice that $\rho(x, y) = \rho(-x, -y)$ if the trapping potential $V(x)$ is an even function; therefore, in such a case the natural orbitals can be chosen to have definite parity. It turns out that they have the same parity as the single-particle wave functions, i.e., $\varphi_j(-x) = (-1)^j \varphi_j(x)$. Then the sum in Eq. (29) is restricted only to even j. For even j the integrals form a decreasing sequence,

$$M_0 > M_2 > M_4 > \cdots, \quad (30)$$

where the $j = 0$ term is typically an order of magnitude greater than $j = 2$, which is, in turn, an order of magnitude greater than the $j = 4$ term, and so on. (From hereafter the differences are not that big, but there is still an ordering.) In Fig. 1 we plot, as an example, the ratios $\frac{M_j}{M_0}$ for the quartic potential and even values of $j = 2, 4, \ldots$. In the inset there is the plot done for the half harmonic oscillator for every j (note the different scales of the two plots). From these figures one can argue that the ordering in (30) is indeed valid.

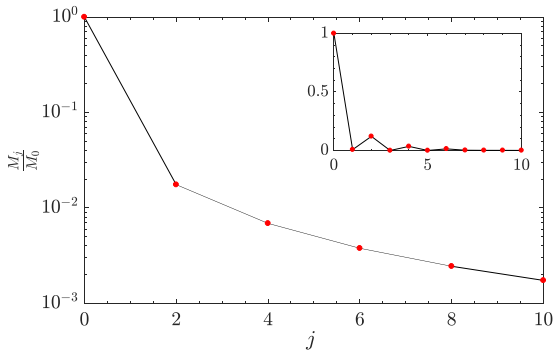

FIG. 1. Ratio M_j/M_0 vs j for the x^4 potential with $N = 25$ for the first 10 even values of j. The plot is in log-scale. In the inset there is found the same ratio evaluated for the half-harmonic oscillator, for every j, with $N = 25$ in linear scale.

To further support this argument, we have also performed an analysis of the coefficients $c_{i,j}$ entering the expansion of the natural orbitals in terms of the single-particle eigenfunctions

$$\varphi_i(x) = \sum_j c_{i,j}\,\phi_j(x). \tag{31}$$

Since both the sets are orthonormal, the coefficients above have to satisfy

$$\sum_j |c_{i,j}|^2 = 1. \tag{32}$$

In Fig. 2 we plot, as an example, the results for the square of the absolute value of the first Fourier coefficients, weighting the first 20 eigenfunctions for the $V(x) \propto x^4$ potential.

We conclude that one can write

$$n_{\text{peak}} \approx \frac{\lambda_0}{2\pi} M_0. \tag{33}$$

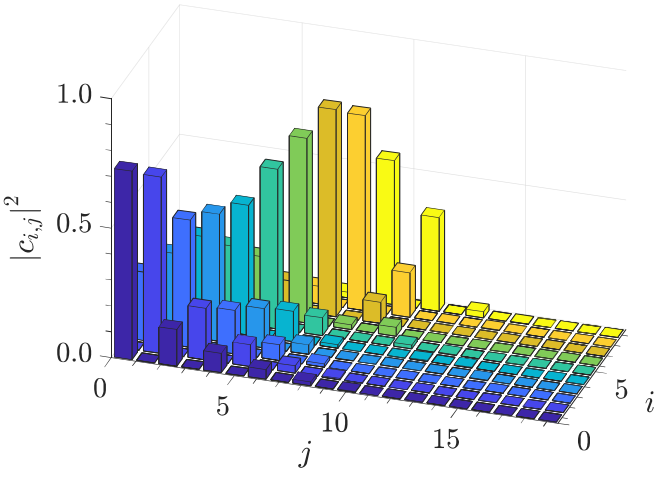

FIG. 2. First ten absolute value squared Fourier coefficients $c_{i,j}$ from (31) weighting the first 20 eigenfunctions for the x^4 potential case, i.e., $i = 0, \ldots, 9$ and $j = 0, \ldots, 19$ ($N = 8$). We have explicitly checked that (32) is satisfied up to 1% error.

C. Scaling laws

In this section we aim to determine a relation between the scaling of the largest eigenvalue of the OBDM and the momentum distribution peak. For this purpose, we have studied the behavior of the natural orbitals $\varphi_j(x)$ for a variety of potentials, including the (even) power-law potentials $V(x) \propto x^{2n}$ and the (non-even) half-harmonic potential $V_{hho}(x)$ defined by $V_{hho}(x) \propto x^2$ for $x > 0$ and $V_{hho}(x) = \infty$ for $x \leqslant 0$. Due to their normalization, the natural orbitals converge for large values of N to certain functions when the position coordinate x is rescaled by a quantity which depends on (and scales with) N.

More precisely, we start by rescaling the position coordinate x in terms of a unit length ξ (see Sec. IV for a definition of ξ in our setup) as

$$\eta \equiv \frac{x}{\xi}. \tag{34}$$

We then define the dimensionless ground-state natural orbital $\hat{\varphi}_0(\eta)$ such that

$$\int |\hat{\varphi}_0(\eta)|^2\, d\eta = 1. \tag{35}$$

It follows that $\hat{\varphi}_0(\eta) \equiv \varphi_0(x)\sqrt{\xi}$. We denote by β the exponent with which $\hat{\varphi}_0(\eta)$ scales with $\hbar$, i.e., $\hat{\varphi}_0(\eta) \sim \hbar^{-\beta}$; in the semiclassical limit this is equivalent [see Eq. (19)] to

$$\hat{\varphi}_0(\eta) \sim N^{\beta}. \tag{36}$$

We have verified that, plotting $\hat{\varphi}_0(\eta)/N^{\beta}$ as a function of $\eta N^{2\beta}$, for $N \to \infty$ the curves converge to a smooth function. In Fig. 3 we plot $\hat{\varphi}_0(\eta)/N^{\beta}$ with respect to $\eta N^{2\beta}$ for the cases of the harmonic potential (top plot) and quartic potential (bottom plot) for different values of the particle number. The convergence to a limiting curve for large N is evident from the figures.

We can also similarly define the dimensionless momentum distribution n_{peak}/ξ and the exponent γ of its scaling with N (or equivalently, $\hbar^{-1}$)

$$\frac{n_{\text{peak}}}{\xi} \sim N^{\gamma}. \tag{37}$$

From Eq. (36), it should be clear that $\int d\eta\, \hat{\varphi}_0(\eta)$ must scale as $N^{-\beta}$ for large N, in such a way that the normalization condition in Eq. (35) continues to hold. In other words, the support of the function $\hat{\varphi}_0(\eta)$ should scale as $N^{-2\beta}$ (see again Fig. 3). From Eqs. (33) and (25) we conclude

$$\frac{n_{\text{peak}}}{\xi} \sim N^{1/2-2\beta}. \tag{38}$$

In particular, from Eq. (38) it follows a scaling law among the exponents γ [defined in Eq. (37)], β [defined in Eq. (36)], and $\mathcal{C}$ [given in Eq. (3)]:

$$\gamma + 2\beta = \mathcal{C}. \tag{39}$$

We will present a numerical check of these results in Sec. IV, in particular, the scaling law (39) for polynomial potentials $V(x) = \Lambda x^{2n}$ with different values of n. A prediction for γ and β for such external trapping potentials will be given at the end of Sec. IV. For the harmonic potential ($n = 1$), from analytical calculations it is already known [22,30] that $\mathcal{C} =$

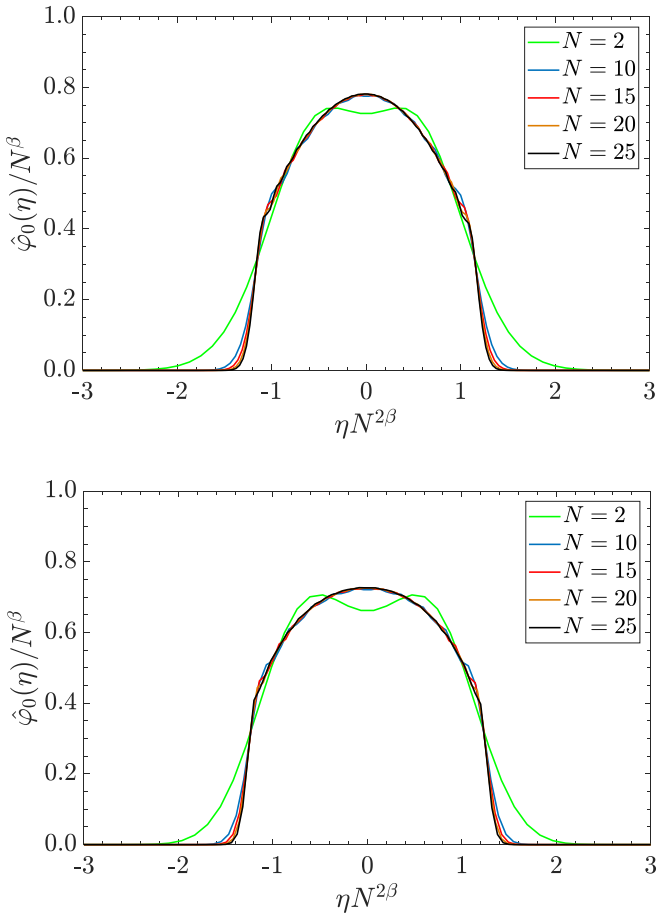

FIG. 3. $\hat{\varphi}_0(\eta)/N^\beta$ vs $\eta N^{2\beta}$ for the harmonic potential ($n = 1$) on the top and the quartic potential ($n = 2$) on the bottom. From the external curve towards the center of both figures, we consider $N = 2, 10, 15, 20, 25$.

$\frac{1}{2}$, $\beta = -\frac{1}{4}$, and $\gamma = 1$, which indeed satisfy both Eqs. (25) and (39).

IV. RESULTS FOR POWER-LAW POTENTIALS

A. Outline of the numerical technique

In Sec. II we have derived an expression for the OBDM of a TG gas in a generic external potential, which leads to Eq. (14). In the following, we are going to study the scaling with the particle number of the OBDM maximum eigenvalue λ_0. For simplicity, we are going to analyze a TG gas at zero temperature trapped by a potential of the form

$$V(x) = \Lambda\, x^{2n}, \tag{40}$$

with n a positive integer and Λ a positive coefficient.

Substituting Eq. (40) into Eq. (8), one gets a single-particle Hamiltonian with a discrete spectrum, and in particular,

$$\left(-\frac{\hbar^2}{2m}\frac{\partial^2}{\partial x^2} + \Lambda\, x^{2n}\right)\phi_k(x) = \varepsilon_k \phi_k(x), \tag{41}$$

for $k = 0, \ldots, N-1$. It is useful to introduce a length scale ξ through

$$\xi = \left(\frac{\hbar^2 b_n}{m\Lambda}\right)^{\frac{1}{2(n+1)}}, \tag{42}$$

where b_n is a numerical constant that we will fix later. Analogously, we define the energy scale $\epsilon \equiv \hbar^2/(m\xi^2)$ and $\eta = \frac{x}{\xi}$ [see Eq. (34)], and then rewrite the single-particle Schrödinger equation as

$$\left[-\frac{1}{2}\frac{\partial^2}{\partial\eta^2} + b_n\,\eta^{2n}\right]\hat{\phi}_k(\eta) = \frac{\varepsilon_k}{\epsilon}\hat{\phi}_k(\eta). \tag{43}$$

To evaluate the OBDM it is needed to determine the single-particle wave functions, solutions of Eq. (43), and substitute their expressions into Eq. (14). The exact analytical solution of the Schrödinger equation (43) is available only for two cases, $n = 1$ and $n = \infty$, that correspond to the harmonic potential and the hard wall, respectively. For intermediate values of n, one has to rely either on numerical methods or the semiclassical WKB approximation, and, as a matter of fact, we have implemented both methods.

We used the lowest order WKB approximation, WKB_0, according to the notation of [56]. One gets then the following estimate for the energy levels of the potential (40) directly from the Bohr-Sommerfeld quantization condition:

$$\varepsilon_k^{wkb} = \left[\sqrt{\frac{\pi}{2m}}\,\frac{\Gamma\left(\frac{3}{2}+\frac{1}{2n}\right)}{\Gamma\left(1+\frac{1}{2n}\right)}\,\hbar\,\Lambda^{1/2n}\right]^{\frac{2n}{n+1}}\left(k+\frac{1}{2}\right)^{\frac{2n}{n+1}}, \tag{44}$$

where $\Gamma(z)$ is the Euler Γ function. From Eq. (42), recalling the definition of the length scale ξ, we obtain

$$\epsilon = \left[\frac{\hbar}{\sqrt{m}}\left(\frac{\Lambda}{b_n}\right)^{\frac{1}{2n}}\right]^{\frac{2n}{n+1}}. \tag{45}$$

We choose then b_n in Eq. (42) in such a way that the energy scale in Eq. (45) matches with the first factor of Eq. (44), namely,

$$b_n = \left[\sqrt{\frac{2}{\pi}}\,\frac{\Gamma\left(1+\frac{1}{2n}\right)}{\Gamma\left(\frac{3}{2}+\frac{1}{2n}\right)}\right]^{2n}. \tag{46}$$

We have checked (44) for different values of n, comparing the semiclassical results with numerical outcomes obtained with the routine CHEBFUN [57] (and also with direct diagonalization of the single-particle Hamiltonian). As one can see from Table I and as expected, the WKB formula [Eq. (44)] approaches the numerical results in the limit of large k (apart from, of course, the harmonic potential case where it is exact). The WKB approximation also provides a form for the single-particle wave functions $\hat{\phi}_k(\eta)$ along the full real line. Near the turning points of the potential, one has to use a standard Airy function approximation.

Since the WKB approximation works better for higher energy levels, as one may check comparing the differences $\varepsilon_k^{wkb} - \varepsilon_k^{num}$ for different values of k, we expect that the value of $\mathcal{C}^{wkb}$ may be be different from the one obtained by numerically computing the single-particle wave functions if N is not very large. Moreover, since the ground state and

TABLE I. Semiclassical energy levels obtained from (44) and the corresponding numerical results for ε_k for $n = 2, 3, 4$ and $V(\eta) = b_n\,\eta^{2n}$, with b_n fixed by (46). Energies are in units of ϵ.

	$n=2$		$n=3$		$n=4$	
k	ε_k^{wkb}	ε_k^{num}	ε_k^{wkb}	ε_k^{num}	ε_k^{wkb}	ε_k^{num}
0	0.397	0.485	0.353	0.505	0.330	0.530
1	1.717	1.739	1.837	1.915	1.913	2.059
2	3.393	3.412	3.953	4.006	4.332	4.435
3	5.314	5.329	6.548	6.593	7.421	7.509
4	7.429	7.442	9.546	9.586	11.09	11.17
5	9.708	9.720	12.89	12.93	15.30	15.37
6	12.13	12.14	16.57	16.61	19.98	20.05
7	14.68	14.69	20.54	20.57	25.12	25.19
8	17.35	17.35	24.78	24.81	30.69	30.75
9	20.12	20.13	29.28	29.31	36.67	36.73
10	22.99	23.00	34.02	34.05	43.04	43.10

first excited-state energies computed with the WKB method, for $n \neq 1$, are smaller than those computed numerically, we expect that the WKB ground state will be more populated by the particles with respect to the exact occupation. Therefore a larger value of $\mathcal{C}^{wkb}$ may be obtained for the values of N we consider ($N \lesssim 30$), which is indeed what we find below.

After determining the single-particle wave functions either numerically or within the WKB approximation, we have generated the OBDM (14) for the potentials in Eq. (40). For $n = 1$ and $n = \infty$ the exact forms of the wave functions are, of course, available and the task simplifies. Finally, we are left with the eigenvalue problem

$$\int \rho(x, y)\,\varphi_j(y)\,dy \;=\; \lambda_j\,\varphi_j(x), \tag{47}$$

that we have solved by discretizing the integral; for finite n, for instance, one can employ a Gauss-Hermite quadrature [58] (see also the Appendix A for more details). To be sure that the method works accurately for different potentials and particle numbers, we have verified whether the results converge, increasing the number of nodes (points) of the quadrature.

We are interested in the study of deviations from ODLRO, and therefore we focus our attention on the behavior of λ_0 for different numbers of particles in the system. To characterize and quantify these deviations in the TG gas, we have fitted the large N asymptotic of the maximum eigenvalue of the OBDM with a power law [22],

$$\lambda_0 \;=\; \mathcal{A} + \mathcal{B}\,N^{\mathcal{C}} + \frac{\mathcal{D}}{N^{\mathcal{E}}}, \tag{48}$$

where in principle all the parameters $\mathcal{A}, \ldots, \mathcal{E}$ are potential dependent (i.e., n dependent). Since the number of particles N typically goes from 2 to 25, subleading finite-size corrections are taken into account by the exponent $\mathcal{E}$ (and the prefactor $\mathcal{D}$) in Eq. (48).

As discussed in the Introduction, it is possible to define two different scalings of λ_0 with respect to the particle number. In the first case [case (b)], we could fix the external potential and increase N. In the second case [case (a)] we could fix instead the density of particles in the trap and vary N and Λ accordingly. For example, for the harmonic potential we can write $\Lambda = \frac{1}{2}\,m\,\omega^2$, and, using the length scale $\xi \equiv \sqrt{\hbar/m\omega}$, we can define the average density $\rho = N/\sqrt{\hbar/m\omega}$. We are going to approach the problem in both ways.

A power-law scaling similar to Eq. (48) can be also argued for the dimensionless momentum distribution peak

$$\frac{n_{\rm peak}}{\xi} \;=\; \mathcal{F} + \mathcal{G}\,N^{\gamma} + \frac{\mathcal{H}}{N^{\mathcal{I}}}. \tag{49}$$

To obtain β defined in (36), we proceed in the following way. First we evaluate $\hat{\varphi}_0(\eta)$ for two different values of the particle number, N_1 and N_2. To have an estimate of β, we impose that

$$\hat{\varphi}_0^{(N_1)}(\eta)\,N_1^{-\beta} \;=\; \hat{\varphi}_0^{(N_2)}(\eta)\,N_2^{-\beta} \tag{50}$$

near the origin, from which it follows that

$$\beta \;=\; \frac{\ln\left[\hat{\varphi}_0^{(N_2)}(\eta)\,/\,\hat{\varphi}_0^{(N_1)}(\eta)\right]}{\ln(N_2/N_1)}. \tag{51}$$

Once the value of β is found, we have checked that the scaled natural orbitals, i.e., $\hat{\varphi}_0(\eta)\,N^{-\beta}$, converge by increasing N.

B. Semiclassical (CFT) determination of the prefactor $\mathcal{B}$ in Eq. (3)

Let us now show how it is possible to use the asymptotic form in Eq. (20) for the OBDM to extract directly the potential-dependent coefficient $\mathcal{B}$ in Eq. (48) for $N \to \infty$ [see Eq. (25)]. Once again, we focus on power-law potentials given in Eq. (40). In the semiclassical limit defined in Eq. (16), the following dimensionful quantities (μ, Λ, m) do not scale with $\hbar$, and we replace them with $(R, \tilde{L}, m)$, where $R \equiv (\frac{\mu}{\Lambda})^{1/2n}$ is a length scale and $\tilde{L}$ the time scale in Eq. (22). For the power-law potentials

$$\tilde{L} = \Xi R\sqrt{\frac{m}{2\mu}}, \tag{52}$$

where Ξ is a numerical constant given by

$$\Xi = \int_{-1}^{1} \frac{du}{\sqrt{1-u^{2n}}} = 2\sqrt{\pi}\,\frac{\Gamma\left(\frac{2n+1}{2n}\right)}{\Gamma\left(\frac{n+1}{2n}\right)}. \tag{53}$$

In the semiclassical approximation $\hbar$ can be replaced by N according to Eq. (19), which in our case reads

$$N\hbar = \frac{mR^2}{\tilde{L}}\left(\frac{\alpha\,\Xi}{\pi}\right). \tag{54}$$

In Eq. (54), α is another numerical constant given by

$$\alpha = \int_{-1}^{1} du\,\sqrt{1-u^{2n}} = \sqrt{\pi}\,\frac{\Gamma\left(\frac{2n+1}{2n}\right)}{\Gamma\left(\frac{3n+1}{2n}\right)}. \tag{55}$$

The OBDM in Eq. (20) is expressed in terms of a variable $\tilde{x}(x) \equiv \tilde{L}\,F(x/R)$. Again, for the potentials in Eq. (40), F is given by

$$F(\eta) \;=\; \frac{1}{\Xi}\int_{-1}^{\eta} du\,\frac{1}{\sqrt{1-u^{2n}}}. \tag{56}$$

However, it is actually more convenient to introduce $G(\eta)$ in such a way that $F(\eta) \equiv \frac{1}{2} + G(\eta)$ and it turns out

$$G(\eta) = \mathrm{sgn}(\eta)\frac{B_{\eta^{2n}}\left(\frac{1}{2n}, \frac{1}{2}\right)}{2n\,\Xi}, \tag{57}$$

where the function $B_z(a, b)$ is the incomplete Beta function [59]. The function $G(\eta)$ simplifies in the limit $n = 1$ (harmonic oscillator), where we have $G(\eta)|_{n=1} = \frac{1}{\pi}\arcsin(\eta)$, and also in the limit $n \to \infty$ (hard wall) where $G(\eta)|_{n=\infty} = \frac{1}{2}\eta$. Taking into account all of this, we can rewrite the eigenvalue equation (2) for the semiclassical OBDM as

$$X\sqrt{N}|C|^2\sqrt{\frac{\pi}{\alpha\,\Xi}}\int_{-1}^{1} d\eta'\, K(\eta, \eta')\varphi_j(\eta') = \lambda_j\varphi_j(\eta), \tag{58}$$

where $K(\eta, \eta')$ is the kernel

$$K(\eta, \eta') = \frac{|1 - \sin^2(\pi G(\eta))|^{\frac{1}{8}}\ |1 - \sin^2(\pi G(\eta'))|^{\frac{1}{8}}}{|\sin(\pi G(\eta)) - \sin(\pi G(\eta'))|^{\frac{1}{2}}}. \tag{59}$$

As already anticipated, the existence of the limit (16) requires $\lambda_j \sim \mathcal{B}_j\sqrt{N}$, i.e., $\mathcal{C} = 1/2$ [see Eq. (48)]. The numerical prefactors $\mathcal{B}_j$ can be calculated from the knowledge of the eigenvalues $\bar{\lambda}_j$ of Eq. (59). Indeed, from (58) one has

$$\mathcal{B}_j \equiv |C|^2\sqrt{\frac{\pi}{\alpha\,\Xi}}\bar{\lambda}_j. \tag{60}$$

In the following we only focus on the scaling of the largest eigenvalue λ_0 and then define $\mathcal{B} \equiv \mathcal{B}_0$, consistently with Eq. (3).

The largest eigenvalue of the kernel in Eq. (59) can be obtained with a numerical procedure similar to that outlined at the end of the previous section. Notice that the kernel in Eq. (59) is singular for $\eta = \eta'$ and its diagonal elements have to be regularized with a cutoff δ. The physical origin of the cutoff can be traced back to the validity of Eq. (20) up to distances $|x - y| \simeq \rho_{\max}^{-1}$. In the dimensionless variable η, therefore the cutoff is $\delta \simeq \frac{\rho_{\max}^{-1}}{R} \ll 1$. This condition, determining the validity of the CFT approach, already appears in [49]. From this perspective the semiclassical limit $\hbar \to 0$ in Eq. (16) it is actually a convenient way to take the continuum limit to a field theory. Such a field theory describes the gas density fluctuations on intermediate length scales much larger than $\rho_{\max}^{-1}$ and much smaller than the effective length R of the system [49,50,54]. A nontrivial consequence is that the two procedures (a) and (b) to implement the large-N limit should reproduce the same results. Indeed, fixing the external potential and varying the density is equivalent to considering $\rho_{\max}^{-1} \to 0$ while keeping R fixed; on the other hand, fixing the density and varying the potential corresponds to $R \to \infty$ while keeping $\rho_{\max}$ fixed. In both cases $\delta \ll 1$ and the gas is described by a CFT.

Numerical estimations for $\mathcal{B}$ in Eq. (60) obtained with a Gauss-Legendre quadrature up to $Z = 20\,000$ nodes are given in Table II and Fig. 4. Z is the number of points of the grid in which the interval $[-1, 1]$ is divided. The error is estimated by extrapolating the value of $\mathcal{B}$ in the limit $\delta \to 0$ by increasing Z. Then the obtained values for varying Z are fitted with a function of the form $\mathcal{B} + \mathcal{M}/Z^{\zeta}$. We observe that

TABLE II. Estimation of the prefactor $\mathcal{B}$ in Eq. (3). The values $\mathcal{B}_{\mathrm{fit}}$ are obtained by fitting the finite-N results for the largest eigenvalue of Eq. (14) with Eq. (48). The fit for λ_0 is done by fixing the potential and varying the density by increasing the number of particles. The numerical error in the last digit is reported in brackets. In the second column are given the values of $\mathcal{B}$ obtained from Eq. (60), after determining numerically the largest eigenvalue $\bar{\lambda}_0$ of the kernel in Eq. (59).

n	$\mathcal{B}_{\mathrm{fit}}$	$\mathcal{B}$
1	1.4304(2)	1.430(4)
2	1.400(4)	1.392(4)
3	1.380(4)	1.378(3)
4	1.372(5)	1.368(2)
∞	1.31(1)	1.308(3)

Refs. [22,60] also provide a numerical evaluation of $\mathcal{B}$ for the harmonic potential ($n = 1$) and the hard wall ($n = \infty$). Our results fully confirm and generalize these predictions.

The CFT predictions for $\mathcal{B}$ are compared in Table II with $\mathcal{B}_{\mathrm{fit}}$, which is the value of $\mathcal{B}$ obtained from the fit (48) using the numerical results for the OBDM $\rho(x, y)$ directly computed. The large-N limit is implemented here, fixing the potential and varying the density [case (b)]. Notice that in doing the fit one could either fix $\mathcal{C}$ to the value $1/2$ or refit $\mathcal{C}$ as well according to (48). Since the value $\mathcal{C} = 1/2$ has been independently established and checked, we present our results for $\mathcal{B}_{\mathrm{fit}}$ with the former procedure. When instead $\mathcal{C}$ is refitted, substantial agreement for $\mathcal{B}_{\mathrm{fit}}$ is found, except for $n \sim 2$–4, where we obtained a discrepancy of order 1%. To check which procedure is better, we performed both with N up to 30, and then we compared their predictions with the value for λ_0 obtained for $N = 35$ directly from the numerical diagonalization of the ODBM. We found that the procedure in which $\mathcal{C}$ is fixed gives slightly better results. Finally, we also verified that the scaling of the largest eigenvalue obtained by fixing the density in the trap and varying the potential [case (a)] is also consistent with the CFT predictions; see

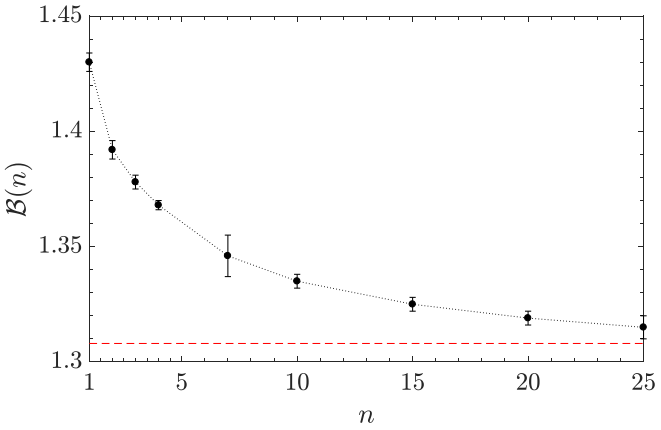

FIG. 4. $\mathcal{B}(n)$ vs n obtained from solving Eq. (58) with kernel given by Eq. (59). $\mathcal{B}$ monotonically decreases from 1.430(4) for $n = 1$ to 1.308(3) for $n = \infty$, which is represented by the red dashed line. The black dotted line is a guide for the eye.

TABLE III. Results for the parameters entering Eq. (48) for different values of n by fixing the trapping potential and varying the density at the center of the trap. The numerical error in the last digit is reported in brackets.

n	$\mathcal{A}_{\rm fit}$	$\mathcal{B}_{\rm fit}$	$\mathcal{D}_{\rm fit}$	$\mathcal{E}_{\rm fit}$
1	$-0.554(2)$	1.4304(2)	0.122(1)	0.60(1)
2	$-0.55(4)$	1.400(4)	0.141(8)	0.79(6)
3	$-0.53(3)$	1.380(4)	0.16(2)	1.1(5)
4	$-0.56(3)$	1.372(5)	0.20(1)	0.9(3)
∞	$-0.6(1)$	1.31(1)	0.31(9)	0.3(1)

Table VI for fits without fixing $\mathcal{C} = 1/2$ and Table VII for fits with $\mathcal{C} = 1/2$. Compare, in particular, the results in Table VII with those collected in Table III. In conclusion, the agreement between the predictions obtained from the CFT formula (20) and the numerical values for $\mathcal{B}_{\rm fit}$ is very satisfactory.

C. Numerical results

Let us now describe the outcome of the numerical analysis, based on Eqs. (48) and (49), for the large-N behavior of λ_0, $n_{\rm peak}/\xi$, and $\hat{\varphi}_0(\eta)$. Such a study strongly corroborates the validity of Eqs. (25) and (39). To obtain the results in Tables III, IV, and V, we have varied the density of particles in the system (by increasing N typically up to 25–30) for different power-law potentials in Eq. (40). In particular, in Table III are collected the results obtained for the parameters of the scaling of λ_0 according to Eq. (48), in Table IV we report the results for the dimensionless momentum distribution peak according to Eq. (49), and in Table V we summarize the values of $\mathcal{C}$, β, and γ obtained as a function of n.

Our findings for λ_0 as a function of N using Eq. (48) are plotted for different values of n in Fig. 5. The inset of Fig. 5 shows the WKB approximation results, where it is called λ_0^{wkb}. The exponent $\mathcal{C}$ is approaching $1/2$ within the numerical error. Also, notice from Table V that $\mathcal{C}^{wkb}$ is greater than $\mathcal{C}_{\rm fit}$ for $n \neq 1$, as expected, and $\mathcal{C} = 1/2$ is within the estimated error for $\mathcal{C}^{wkb}$ (but $n = 2$).

By studying the system by fixing the density and varying Λ, we have collected the data reported in Table VI for different values of n of the polynomial trapping potential. From these results is evident that $\mathcal{C} = 1/2$ is also found in this case. For this reason we then fitted the data via Eq. (48) with $\mathcal{C}$ fixed to the value $1/2$ and we obtained the results reported in Table VII. Consistently with the discussion in Sec. IV B, the values estimated for the parameter $\mathcal{B}$ (actually for all the fit parameters) are consistent within the error bar with the ones in Table III.

TABLE IV. Results for the parameters in the dimensionless momentum distribution peak (49) for different values of n. Note that for $n = 1$ the correction term $\propto 1/N$ in the fitting is not necessary.

n	$\mathcal{F}_{\rm fit}$	$\mathcal{G}_{\rm fit}$	$\mathcal{H}_{\rm fit}$	$\mathcal{I}_{\rm fit}$
1	0.002(2)	0.561(6)		
2	$-0.046(8)$	0.5001(3)	0.025(6)	0.6(3)
3	$-0.15(8)$	0.491(2)	0.10(8)	0.3(3)
4	$-0.21(1)$	0.500(5)	0.015(5)	0.41(3)
∞	$-0.752(3)$	0.1994(2)	0.0048(1)	1.09(5)

TABLE V. From the second to the fifth columns are gathered numerical results for the parameters ruling the scaling with N of λ_0, λ_0^{wkb}, $\hat{\varphi}_0(\eta)$, and $n_{\rm peak}/\xi$. The value for $\mathcal{C}$, within numerical precision, appears to be independent of the potential and equal to $1/2$. Last two columns: Exact values for β and γ coming from Eqs. (69) and (70), respectively.

n	$\mathcal{C}_{\rm fit}$	$\mathcal{C}^{wkb}$	$\beta_{\rm fit}$	$\gamma_{\rm fit}$	β	γ
1	0.500(2)	0.496(8)	$-0.25(1)$	1.02(4)	$-\frac{1}{4}$	1
2	0.501(1)	0.54(3)	$-0.16(1)$	0.85(2)	$-\frac{1}{6}$	$\frac{5}{6}$
3	0.501(2)	0.54(7)	$-0.12(2)$	0.76(1)	$-\frac{1}{8}$	$\frac{3}{4}$
4	0.500(3)	0.54(9)	$-0.10(1)$	0.70(1)	$-\frac{1}{10}$	$\frac{7}{10}$
∞	0.500(1)		0.00(1)	0.502(2)	0	$\frac{1}{2}$

We have also done calculations for a potential $V_{hho}(x) = \Lambda x^2$ for $x > 0$ and zero otherwise, i.e., half of the harmonic potential. By varying the density in the system we get

$$\mathcal{A}_{\rm fit} = -0.37(1);\ \ \mathcal{B}_{\rm fit} = 1.267(3);\ \ \mathcal{C}_{\rm fit} = 0.51(2);$$
$$\mathcal{D}_{\rm fit} = 0.103(1);\ \ \mathcal{E}_{\rm fit} = 0.58(1). \tag{61}$$

D. The hard wall potential

The case of $n = \infty$ is analogous to impose Dirichlet boundary conditions (DBC) and the situation is slightly different than the previous cases. In this case, one has to evaluate

$$\int_0^L \rho(x, y)\, \varphi_j(y)\, dy \;=\; \lambda_j\, \varphi_j(x), \tag{62}$$

so that the Gauss-Hermite quadrature cannot be applied anymore. We rather used the Gauss-Legendre quadrature, see Appendix A. The same will happen with periodic bound-

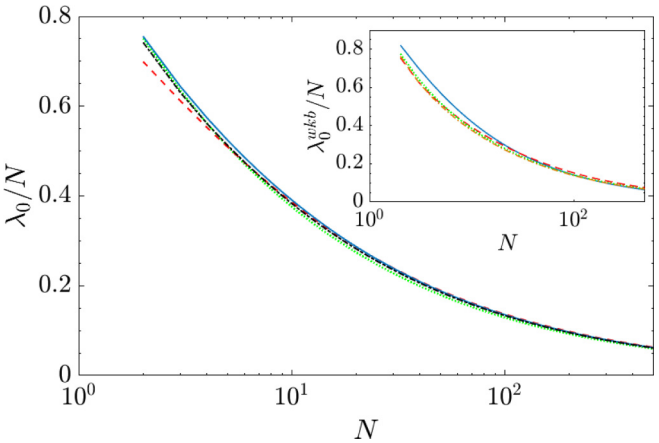

FIG. 5. λ_0 vs N obtained for $n = 1$ (in solid blue), $n = 2$ (in dashed red), $n = 3$ (in dotted green), and $n = \infty$ (in dotted-dashed black), up to 500 particles. In the inset is shown the behavior of λ_0^{wkb} vs N obtained with the WKB approximation, for $n = 1$ (in solid blue), $n = 2$ (in dashed red), $n = 3$ (in dotted green), and $n = 4$ (in dotted-dashed orange).

TABLE VI. Results for the parameters entering Eq. (48) for different values of n by fixing the density at the center of the traps and varying N and Λ accordingly. The numerical error in the last digit is reported in brackets.

n	$\mathcal{A}_{\rm fit}$	$\mathcal{B}_{\rm fit}$	$\mathcal{C}_{\rm fit}$	$\mathcal{D}_{\rm fit}$	$\mathcal{E}_{\rm fit}$
1	−0.58(2)	1.45(3)	0.4995(8)	0.36(5)	2.00(1)
2	−0.56(3)	1.418(2)	0.498(5)	0.16(4)	1.2(3)
3	−0.56(2)	1.391(1)	0.500(3)	0.18(2)	1.0(1)
4	−0.52(7)	1.34(4)	0.503(6)	0.21(1)	0.30(5)

ary conditions (PBCs) and Neumann boundary conditions (NBCs). In these cases Vandermonde determinant formulas can be used to get closed expressions for the OBDM [44], which are easier to handle numerically for large number of particles [still the formula (14) can be used]. Therefore one just needs to construct the entire OBDM, varying $\theta = \pi x/L$ and $\sigma = \pi y/L$ from 0 to π, and directly diagonalize the finite-dimensional matrix after the discretization. With these three different boundary conditions we got the following results:

(1) PBC: Using the results in [6], we can compute the eigenvalues of the OBDM for a TG gas in a circular geometry up to 10^3 particles. In this case the best fitting law is the one not having the correction term $\propto 1/N$ in (48), since we work with a very large number of particles. In this case we have

$$\mathcal{A}_{\rm fit} = -0.597(1);\ \ \mathcal{B}_{\rm fit} = 1.4741(1);$$
$$\mathcal{C}_{\rm fit} = 0.5000(1). \tag{63}$$

Fixing $\mathcal{C} = 1/2$ in the fitting procedure, one gets

$$\mathcal{A}_{\rm fit} = -0.602(1);\ \ \mathcal{B}_{\rm fit} = 1.475(1). \tag{64}$$

(2) DBC ($n = \infty$): With the hard wall potential with $b_\infty = 0$ from (46), we have considered values of N up to $N = 150$. The corresponding results for λ_0 are presented in Tables III and V, and those for the momentum distribution in Table IV. For the natural orbitals we found that they are independent of N, i.e., $\beta = 0$.

(3) NBC: In this case we computed the OBDM and its eigenvalues up to 100 particles. Fitting via Eq. (48), we have

$$\mathcal{A}_{\rm fit} = -0.71(1);\ \ \mathcal{B}_{\rm fit} = 1.340(4);\ \ \mathcal{C}_{\rm fit} = 0.497(5);$$
$$\mathcal{D}_{\rm fit} = 0.482(7);\ \ \mathcal{E}_{\rm fit} = 1.33(5). \tag{65}$$

Fixing $\mathcal{C} = 1/2$ during the fitting procedure, we get

$$\mathcal{A}_{\rm fit} = -0.68(5);\ \ \mathcal{B}_{\rm fit} = 1.32(1);$$
$$\mathcal{D}_{\rm fit} = 0.49(7);\ \ \mathcal{E}_{\rm fit} = 1.6(2). \tag{66}$$

TABLE VII. Results for the parameters entering Eq. (48) with $\mathcal{C}$ fixed to 1/2 for different values of n by fixing the density at the center of the traps and varying N and Λ accordingly. The numerical error in the last digit is reported in brackets.

n	$\mathcal{A}_{\rm fit}$	$\mathcal{B}_{\rm fit}$	$\mathcal{D}_{\rm fit}$	$\mathcal{E}_{\rm fit}$
1	−0.56(3)	1.432(4)	0.13(3)	0.57(2)
2	−0.55(2)	1.407(4)	0.15(3)	1.0(2)
3	−0.56(2)	1.391(1)	0.18(2)	1.0(1)
4	−0.56(1)	1.38(2)	0.18(4)	0.8(1)

E. Analytical predictions for β and γ

All previous results are compatible (within the numerical error) with an exponent $\mathcal{C}$, characterizing deviations from ODLRO in the thermodynamic limit, equal to 1/2. For very large numbers of particles we therefore confirm the validity of Eq. (25), independently of the external potential. It is also interesting to observe that not only is Eq. (39) satisfied for the different power-law potentials analyzed, but also that it is possible to work out predictions for β and γ as a function of n. For β one can observe that, recalling the definition of length scale ξ in Eq. (42), the support of the dimensionless ground-state natural orbit scales as ξ^{-1}, i.e.,

$$\int d\eta \propto \frac{1}{\xi} \propto \hbar^{-\frac{1}{n+1}}. \tag{67}$$

Since $\int d\eta \propto N^{-2\beta}$ (see Sec. III) and in the semiclassical limit $\hbar \propto N^{-1}$, then we have

$$N^{-2\beta} \propto N^{\frac{1}{n+1}}, \tag{68}$$

from which

$$\beta = -\frac{1}{2n+2}. \tag{69}$$

From the universal relation (39) it also follows a prediction for γ:

$$\gamma = \frac{n+3}{2(n+1)}. \tag{70}$$

The main results for the exponents $\mathcal{C}$, γ, and β for different power-law potentials are reported in Table V. Hence, the predictions (69) and (70) are in excellent agreement with the numerical results.

Finally, let us observe that the result $\gamma = 1$ for $n_{\rm peak}/\xi$ in the case of harmonic potential does not imply at all that in an experiment one would see a Bose-Einstein condensate (i.e., a macroscopic occupation of the lowest energy state). Indeed, also ξ has a dependence on N. In experiments where $\tilde{\rho}(k)$ is measured, from Eq. (67) one would have

$$n_{\rm peak} \sim N^{1/2}. \tag{71}$$

The same behavior is obtained for all values of n. This shows that for a TG gas the condensate *fraction* is $1/\sqrt{N}$ independently of the external trapping potential used to confine the system.

V. CONCLUSIONS

In this paper we have studied the universal off-diagonal long-range-order behavior for a trapped Tonks-Girardeau gas at zero temperature. First we have focused on the scaling of the largest eigenvalue λ_0 of the one-body density matrix of the gas with respect to its particle number N, defining the exponent $\mathcal{C}$ via the relation $\lambda_0 \sim \mathcal{B}N^{\mathcal{C}}$. For the one-dimensional homogeneous Tonks-Girardeau gas a well-known result is $\mathcal{C} = 1/2$. Here we have investigated the inhomogeneous case and we have showed that $\mathcal{C} = 1/2$ actually characterizes the hard-core system independently of the external trapping potential. We also derived analytical predictions for the prefactor

$\mathcal{B}$. The field theoretical approach on which we relied shows clearly that the large-N asymptotic of the largest eigenvalue of the OBDM is the same, varying the density and fixing the external potential or varying the external potential and fixing the density.

We have then defined the exponents γ and β of the scaling against N of the dimensionless momentum distribution peak and the eigenfunction of the one-body density matrix relative to λ_0, respectively. We have also defined a scaling length ξ, in terms of which we have introduced a dimensionless variable η as $\eta = x/\xi$, further showing that ξ scales with N as $\xi \propto N^{2\beta}$ (the factor 2 is introduced for convenience). The dimensionless ground-state natural orbital is then defined as $\hat{\varphi}_0(\eta) \equiv \varphi_0(x)\sqrt{\xi} \propto \xi^{1/2}$, due to the normalization condition of $\varphi_0(x)$. Therefore, as one inserts more particles into the system, the dimensionless natural orbital corresponding to λ_0 are wider, as expected. It then follows that $\hat{\varphi}_0(\eta) \sim N^{\beta}$. Another power-law scaling can be defined for the dimensionless momentum distribution peak $n_{\rm peak}/\xi \sim N^{\gamma}$. Then we have showed that $\gamma + 2\beta = \mathcal{C}$.

Confining the system in a power-law potential, $V(x) \propto x^{2n}$, we were able to get analytical predictions for β and γ. Using a semiclassical approximation approach, we have found that $\beta = -1/(2n+2)$ and $\gamma = (n+3)/[2(n+1)]$. We provided numerical checks for these predictions, using both a WKB approximation and exact numerical results. We have finally showed that it holds the following power-law scaling for the (dimensionful) momentum distribution peak: $n_{\rm peak} \propto N^{1/2}$, valid for any external power-law potential. This is another universal property for hard-core bosons analogous to that for the largest eigenvalue λ_0. The result for $n_{\rm peak}$ is of interest for experiments, since one has access to momentum distribution profiles, and therefore for a TG gas in a trap a condensate fraction of the order of $1/\sqrt{N}$ would be seen.

As a future work, it would be interesting to study the universal properties of the off-diagonal long-range order for a trapped Lieb-Liniger gas with finite coupling constant.

ACKNOWLEDGMENTS

Discussions and useful correspondence with J. Dubail and P. Calabrese are gratefully acknowledged. G.M. and A.T. are grateful to the Erwin Schrödinger International Institute for Mathematics and Physics (ESI) in Wien for the kind hospitality during the programme "Quantum Paths." J.V. thanks SISSA and INFN for the kind hospitality during the final stage of this work.

APPENDIX: GAUSS QUADRATURE METHOD

The Gauss quadrature rule is a method with which one can estimate in terms of a finite sum an integral of a function $f(x)$ of the form

$$\int_a^b f(x)\, w(x)\, dx, \tag{A1}$$

where $w(x)$ is some weight function. In the Gauss quadrature method the weights and nodes (points) we are evaluating $f(x)$ are chosen in advance. This choice is based on the support of the integral in Eq. (A1). For example, with the Gauss-Hermite quadrature one is able to compute integrals with $a \equiv -\infty$, $b \equiv \infty$ and weight function $w(x) = e^{-x^2}$ in the following way:

$$\int f(x)\, e^{-x^2}\, dx \approx \sum_{i=1}^{Z} w_i\, f(\xi_i), \tag{A2}$$

where the ξ_i's are the roots of the Hermite polynomial $H_Z(x)$, and (A2) is exact for all polynomials $f(x)$ of degree less or equal than $2Z-1$.

For the case of our interest, $f(x) \equiv \rho(x, y)$. In order to recast (47) in the form of (A2), we have to multiply and divide by e^{-y^2}. By choosing $x = \xi_k$, with $k = 1, \ldots, Z$, we have Z equations of the form

$$\int [\rho(\xi_k, y)\, \varphi_j(y)\, e^{y^2}] e^{-y^2}\, dy = \lambda_j\, \varphi_j(\xi_k). \tag{A3}$$

Using (A2) we then have

$$\sum_{i=1}^{Z} w_i\, \rho(\xi_k, \xi_i)\, \varphi_j(\xi_i)\, e^{\xi_i^2} = \lambda_j\, \varphi_j(\xi_k), \tag{A4}$$

providing an eigenvalue equation for a $Z \times Z$ matrix S with entries

$$S_{k,i} = \rho(\xi_k, \xi_i)\, w_i\, e^{\xi_i^2}. \tag{A5}$$

Accordingly, one has to diagonalize this finite-dimensional matrix to obtain the occupation numbers λ_j and the natural orbitals $\varphi_j(x)$. Of course, the larger Z is, the better the approximation results for the integrals. One has to check whether by increasing Z the resulting value for the integral is converging. In the cases considered in the paper, this condition was fulfilled and we used Z ranging from ∼80 to ∼170. Moreover, one has a condition to check, that is,

$$\sum_{j=1}^{Z} \lambda_j = N, \tag{A6}$$

with N the number of particles in the system. If Eq. (A6) is not satisfied, then we have to increase Z.

If the support of the OBDM is compact, as in the case of the CFT limit of Sec. IV B, one can rely on another quadrature scheme. For instance, the Gauss-Legendre quadrature method can be applied to integrals having integration domain $[-1, 1]$ and gives

$$\int_{-1}^{1} f(x)\, dx \approx \sum_{i=1}^{Z} w_i\, f(\xi_i). \tag{A7}$$

For the case of the half-harmonic oscillator, one can use the same procedure but with different weights and nodes. The integration interval is $[0, \infty)$ and one has to apply the Gauss-Laguerre quadrature method:

$$\int_0^{\infty} f(x)\, e^{-x}\, dx \approx \sum_{i=1}^{Z} w_i\, f(\xi_i). \tag{A8}$$

The final form of the $Z \times Z$ matrix S to diagonalize is then

$$S_{k,i} = \rho(\xi_k, \xi_i)\, w_i\, e^{\xi_i}, \tag{A9}$$

for $k, i = 1, \ldots, Z$.

[1] L. P. Pitaevskii and S. Stringari, *Bose-Einstein Condensation and Superfluidity* (Oxford University Press, Oxford, UK, 2016).
[2] O. Penrose and L. Onsager, Phys. Rev. **104**, 576 (1956).
[3] C. N. Yang, Rev. Mod. Phys. **34**, 694 (1962).
[4] A. J. Coleman and V. I. Yukalov, Mod. Phys. Lett. B **5**, 1679 (1991); Nuovo Cimento **107**, 535 (1992).
[5] E. Lieb and W. Liniger, Phys. Rev. **130**, 1605 (1963).
[6] A. Colcelli, G. Mussardo, and A. Trombettoni, Europhys. Lett. **122**, 50006 (2018).
[7] F. D. M. Haldane, Phys. Rev. Lett. **47**, 1840 (1981).
[8] T. Giamarchi, *Quantum Physics in One Dimension* (Oxford University Press, Oxford, UK, 2003).
[9] M. Girardeau, J. Math. Phys. **1**, 516 (1960).
[10] A. Lenard, J. Math. Phys. **5**, 930 (1964).
[11] K. K. Das, M. D. Girardeau, and E. M. Wright, Phys. Rev. Lett. **89**, 170404 (2002).
[12] B. Paredes, A. Widera, V. Murg, O. Mandel, S. Fölling, I. Cirac, G. V. Shlyapnikov, T. W. Hänsch, and I. Bloch, Nature (London) **429**, 277 (2004).
[13] T. Kinoshita, T. Wenger, and D. S. Weiss, Science **305**, 1125 (2004).
[14] E. Haller, M. Gustavsson, M. J. Mark, J. G. Danzl, R. Hart, G. Pupillo, and H.-C. Nägerl, Science **325**, 1224 (2009).
[15] E. Haller, R. Hart, M. J. Mark, J. G. Danzl, L. Reichsöllner, M. Gustavsson, M. Dalmonte, G. Pupillo, and H.-C. Nägerl, Nature (London) **466**, 597 (2010).
[16] G. Boéris, L. Gori, M. D. Hoogerland, A. Kumar, E. Lucioni, L. Tanzi, M. Inguscio, T. Giamarchi, C. D'Errico, G. Carleo, G. Modugno, and L. Sanchez-Palencia, Phys. Rev. A **93**, 011601 (2016).
[17] V. E. Korepin, N. M. Bogoliubov, and A. G. Izergin, *Quantum Inverse Scattering Method and Correlation Functions* (Cambridge University Press, Cambridge, UK, 1993).
[18] F. Franchini, *An Introduction to Integrable Techniques for One-Dimensional Quantum Systems* (Springer, Cham, 2017).
[19] M. D. Girardeau, Phys. Rev. Lett. **97**, 210401 (2006).
[20] M. D. Girardeau and E. M. Wright, Phys. Rev. Lett. **84**, 5691 (2000).
[21] R. Pezer and H. Buljan, Phys. Rev. Lett. **98**, 240403 (2007).
[22] P. J. Forrester, N. E. Frankel, T. M. Garoni, and N. S. Witte, Phys. Rev. A **67**, 043607 (2003).
[23] G. J. Lapeyre, M. D. Girardeau, and E. M. Wright, Phys. Rev. A **66**, 023606 (2002).
[24] A. Minguzzi and D. M. Gangardt, Phys. Rev. Lett. **94**, 240404 (2005).
[25] P. Vignolo and A. Minguzzi, Phys. Rev. Lett. **110**, 020403 (2013).
[26] M. Collura, S. Sotiriadis, and P. Calabrese, Phys. Rev. Lett. **110**, 245301 (2013).
[27] G. Lang, P. Vignolo, and Anna Minguzzi, Eur. Phys. J. Special Topics **226**, 1583 (2017).
[28] M. Rizzi, C. Miniatura, A. Minguzzi, and P. Vignolo, Phys. Rev. A **98**, 043607 (2018).
[29] M. Rigol and A. Muramatsu, Phys. Rev. A **70**, 031603 (2004).
[30] B.-B. Wei, S.-J. Gu, and H.-Q. Lin, Phys. Rev. A **79**, 063627 (2009).
[31] K. Lelas, T. Ševa, H. Buljan, and J. Goold, Phys. Rev. A **86**, 033620 (2012).
[32] Z.-L. Wang, A.-M. Wang, and X.-C. Li, arXiv:1201.6019v2.
[33] F. Cartarius, E. Kawasaki, and A. Minguzzi, Phys. Rev. A **92**, 063605 (2015).
[34] G. E. Astrakharchik, K. V. Krutitsky, M. Lewenstein, and F. Mazzanti, Phys. Rev. A **93**, 021605 (2016).
[35] G. E. Astrakharchik, K. V. Krutitsky, M. Lewenstein, F. Mazzanti, and J. Boronat, Phys. Rev. A **96**, 033606 (2017).
[36] J. Radić, V. Bačić, D. Jukić, M. Segev, and H. Buljan, Phys. Rev. A **81**, 063639 (2010).
[37] R. Seiringer and S. Warzel, New J. Phys. **18**, 035002 (2016).
[38] J. Settino, N. Lo Gullo, A. Sindona, J. Goold, and F. Plastina, Phys. Rev. A **95**, 033605 (2017).
[39] G. E. Astrakharchik, J. Boronat, J. Casulleras, and S. Giorgini, Phys. Rev. Lett. **95**, 190407 (2005).
[40] M. T. Batchelor, M. Bortz, X. W. Guan, and N. Oelkers, J. Stat. Mech. (2005) L10001.
[41] M. Kormos, G. Mussardo, and A. Trombettoni, Phys. Rev. A **83**, 013617 (2011).
[42] M. D. Girardeau and G. E. Astrakharchik, Phys. Rev. Lett. **109**, 235305 (2012).
[43] M. Panfil, J. De Nardis, and J.-S. Caux, Phys. Rev. Lett. **110**, 125302 (2013).
[44] P. J. Forrester, N. E. Frankel, T. M. Garoni, and N. S. Witte, Commun. Math. Phys. **238**, 257 (2003).
[45] G. Marmorini, M. Pepe, and P. Calabrese, J. Stat. Mech. (2016) 073106.
[46] Y. Hao, Phys. Rev. A **93**, 063627 (2016).
[47] M. Campostrini and E. Vicari, Phys. Rev. Lett. **102**, 240601 (2009).
[48] M. Campostrini and E. Vicari, Phys. Rev. A **81**, 023606 (2010); **81**, 063614 (2010).
[49] Y. Brun and J. Dubail, SciPost Phys. **2**, 012 (2017).
[50] J. Dubail, J. M. Stéphan, J. Viti, and P. Calabrese, SciPost Phys. **2**, 002 (2017).
[51] M. A. Cazalilla, R. Citro, T. Giamarchi, E. Orignac, and M. Rigol, Rev. Mod. Phys. **83**, 1405 (2011).
[52] M. D. Girardeau, E. M. Wright, and J. M. Triscari, Phys. Rev. A **63**, 033601 (2001).
[53] P. Forrester, arXiv:1806.10411.
[54] Y. Brun and J. Dubail, SciPost Phys. **4**, 037 (2018).
[55] C. J. Pethick and H. Smith, *Bose-Einstein Condensation in Dilute Gases* (Cambridge University Press, Cambridge, UK, 2008), Chap. 16.
[56] C. M. Bender and S. A. Orszag, *Advanced Mathematical Methods for Scientists and Engineers* (Springer-Verlag, New York, 1999).
[57] *Chebfun Guide*, edited by T. A. Driscoll, N. Hale, and L. N. Trefethen (Pafnuty Publications, Oxford, 2014).
[58] L. M. Delves and J. L. Mohamed, *Computational Methods for Integral Equations* (Cambridge University Press, Cambridge, UK, 1985).
[59] *Handbook of Mathematical Functions: With Formulas, Graphs, and Mathematical Tables*, edited by M. Abramowitz and I. A. Stegun (Dover, New York, 1972).
[60] P. J. Forrester, N. E. Frankel, and T. M. Garoni, J. Math. Phys. **44**, 4157 (2003).